

## Interpreting GEMS geostationary satellite observations of the diurnal variation of nitrogen dioxide (NO<sub>2</sub>) over East Asia

Laura Hyesung Yang<sup>1</sup>, Daniel J. Jacob<sup>1,2</sup>, Ruijun Dang<sup>1</sup>, Yujin J. Oak<sup>1</sup>, Haipeng Lin<sup>1</sup>, Jhoon Kim<sup>3</sup>, Shixian Zhai<sup>4</sup>, Nadia K. Colombi<sup>2</sup>, Drew C. Pendergrass<sup>1</sup>, Ellie Beaudry<sup>1</sup>, Viral Shah<sup>5,6</sup>, Xu Feng<sup>1</sup>, Robert M. Yantosca<sup>1</sup>, Heesung Chong<sup>7</sup>, Junsung Park<sup>7</sup>, Hanlim Lee<sup>8</sup>, Won-Jin Lee<sup>9</sup>, Soontae Kim<sup>10</sup>, Eunhye Kim<sup>10</sup>, Katherine R. Travis<sup>11</sup>, James H. Crawford<sup>11</sup>, Hong Liao<sup>12</sup>

<sup>1</sup> Harvard University, John A. Paulson School of Engineering and Applied Sciences, Cambridge, MA 02138, USA

<sup>2</sup> Harvard University, Department of Earth and Planetary Sciences, Cambridge, MA 01238, USA

<sup>3</sup> Yonsei University, Department of Atmospheric Sciences, Seoul 03722, South Korea

<sup>4</sup> Earth and Environmental Sciences Programme and Graduation Division of Earth and Atmospheric Sciences, Faculty of Science, The Chinese University of Hong Kong, Sha Tin, Hong Kong SAR, China

<sup>5</sup> Global Modeling and Assimilation Office, NASA Goddard Space Flight Center, Greenbelt, MD 20770, USA

<sup>6</sup> Science Systems and Applications, Inc., Lanham, MD 20706, USA

<sup>7</sup> Center for Astrophysics | Harvard & Smithsonian, Cambridge, Massachusetts 02138, USA

<sup>8</sup> Pukyong National University, Division of Earth Environmental System Science, Busan 48513, South Korea

<sup>9</sup> Environmental Satellite Center, National Institute of Environmental Research, Incheon 22689, South Korea

<sup>10</sup> Ajou University, Department of Environmental and Safety Engineering, Suwon 16499, South Korea

<sup>11</sup> NASA Langley Research Center, Hampton, VA 23666, USA

<sup>12</sup> Collaborative Innovation Center of Atmospheric Environment and Equipment Technology/Joint International Research Laboratory of Climate and Environment Change, School of Environmental Science and Engineering, Nanjing University of Information Science and Technology, Nanjing 210044, China

Correspondence to: Laura Hyesung Yang ([laurayang@g.harvard.edu](mailto:laurayang@g.harvard.edu))

**Abstract.** Nitrogen oxide radicals (NO<sub>x</sub> ≡ NO + NO<sub>2</sub>) emitted by fuel combustion are important precursors of ozone and particulate matter pollution, and NO<sub>2</sub> itself is harmful to public health. The Geostationary Environment Monitoring Spectrometer (GEMS), launched in space in 2020, now provides hourly daytime observations of NO<sub>2</sub> columns over East Asia. This diurnal variation offers unique information on the emission and chemistry of NO<sub>x</sub>, but it needs to be carefully interpreted. Here we investigate the drivers of the diurnal variation of NO<sub>2</sub> observed by GEMS during winter and summer over Beijing and Seoul. We place the GEMS observations in the context of ground-based column observations (Pandora instruments) and GEOS-Chem chemical transport model simulations. We find good agreement between the diurnal variations of NO<sub>2</sub> columns in GEMS, Pandora, and GEOS-Chem, and we use GEOS-Chem to interpret these variations. NO<sub>x</sub> emissions are four times higher in the daytime than at night, driving an accumulation of NO<sub>2</sub> over the course of the day, offset by losses from chemistry and transport (horizontal flux divergence). For the urban core, where the Pandora instruments are located, we find that NO<sub>2</sub> in winter

Deleted:

40 increases throughout the day due to high daytime emissions and increasing  $\text{NO}_2/\text{NO}_x$  ratio from  
entrainment of ozone, partly balanced by loss from transport and with negligible role of chemistry. In  
summer, by contrast, chemical loss combined with transport drives a minimum in the  $\text{NO}_2$  column at 13-14  
local time. Segregation of the GEMS data by wind speed further demonstrates the effect of transport, with  
 $\text{NO}_2$  in winter accumulating throughout the day at low winds but flat at high winds. The effect of transport  
45 can be minimized in summer by spatially averaging observations over the broader metropolitan scale, under  
which conditions the diurnal variation of  $\text{NO}_2$  reflects a dynamic balance between emission and chemical  
loss.

### 1. Introduction

The Geostationary Environment Monitoring Spectrometer (GEMS) satellite instrument was launched  
50 in February 2020 by the National Institute of Environmental Research (NIER) to observe air quality over  
East Asia. GEMS is the first geostationary instrument directed at air quality and provides hourly column  
measurements of several gases including nitrogen dioxide ( $\text{NO}_2$ ) (J. Kim et al., 2020).  $\text{NO}_2$  is part of the  
nitrogen oxides ( $\text{NO}_x \equiv \text{NO} + \text{NO}_2$ ) radical family, which is emitted by fuel combustion and whose  
chemistry plays a critical role in driving ozone ( $\text{O}_3$ ) and fine particulate matter ( $\text{PM}_{2.5}$ ) formation.  $\text{NO}_2$   
55 itself is of concern as an air pollutant. Loss of  $\text{NO}_x$  is by atmospheric oxidation by the hydroxyl radical  
(OH) and ozone, resulting in a lifetime of a few hours in summer and about a day in winter (Shah et al.,  
2020). The diurnal cycle of  $\text{NO}_2$  measured from geostationary orbit offers unique information on the  
emission, chemistry, and transport of  $\text{NO}_x$ . Here we interpret the GEMS observations with the GEOS-  
Chem chemical transport model (CTM) to better understand the processes controlling this diurnal cycle.

60 Several studies have examined the diurnal variation of  $\text{NO}_2$  in urban air using surface  
concentrations from air quality networks. The data typically exhibit bimodal maxima in the morning around  
7-9 local time (LT) and in the evening around 19-21 LT, including over Beijing and Seoul (Cheng et al.,  
2018; H. Kim et al., 2020). This has been commonly attributed to high  $\text{NO}_x$  emission during morning and

evening rush hours (Kendrick et al., 2015; Cheng et al., 2018), but urban NO<sub>x</sub> emission inventories show  
65 little variation during daytime (Miao et al., 2020). Moutinho et al. (2020) found that the morning and  
evening NO<sub>2</sub> maxima could be driven by shallow mixing depths, in contrast to the middle of the day and  
afternoon hours when surface heating maximizes the mixing depth. This diurnal maximum in mixing depth  
defines the planetary boundary layer (PBL) in daily contact with the surface. The PBL depth extends  
typically to 1-3 km altitude.

Deleted: where

Deleted: drives deep

Deleted: and

Deleted: depth of the

70 Ground-based measurements of NO<sub>2</sub> columns are available from the Pandora Sun-staring  
spectrometer instrument network used for validating satellite observations (Herman et al., 2009; Kanaya et  
al., 2014; Judd et al., 2020; Verhoelst et al., 2021). Column measurements integrate concentrations from  
the surface to the top of the atmosphere and are therefore not directly sensitive to mixing depth. The  
Pandora network consists mainly of urban sites, where the NO<sub>2</sub> column and its variability are mainly within  
75 the PBL (Yang et al., 2023). The Pandora data from Seoul tend to show an increasing trend in the early  
morning followed by flat concentrations over the rest of the daytime, with less diurnal variation than NO<sub>2</sub>  
concentrations in surface air (Crawford et al., 2021). Nearby sites can show different diurnal variations,  
pointing to a major role of local transport in driving this variation (Chang et al., 2022; S. Kim et al., 2023).

Satellite observations of NO<sub>2</sub> from polar sun-synchronous low-earth orbit (LEO) have been made  
80 since 1995 starting with the GOME instrument (Martin et al., 2002) but observe by design at a single time  
of day. Several studies have combined observations from the SCIAMACHY or GOME-2 instruments  
observing in the morning at 9-10 LT and the OMI instrument observing in the afternoon at 13-14 LT to get  
some information on NO<sub>2</sub> diurnal variation. Boersma et al. (2008) found decreases from morning to  
afternoon over urban regions that they attributed to photochemical loss, and increases from morning to  
85 afternoon over tropical biomass burning regions that they attributed to a midday maximum in emissions.  
Boersma et al. (2009) found that the urban morning-to-afternoon decrease was largest in summer and  
absent in winter. Penn and Holloway (2020) found that NO<sub>2</sub> column ratios between morning and afternoon

were lower than surface NO<sub>2</sub> concentration ratios, as would be expected from deeper vertical mixing in the afternoon. Ghude et al. (2020) found an important role for transport in driving morning-to-afternoon variations in NO<sub>2</sub> columns over urban India. [Edwards et al. \(2024\) found that the diurnal variation of the NO<sub>2</sub> column from GEMS in June is driven by photochemistry at a regional scale and variability in emissions and meteorology at a local scale.](#)

Here we analyze and compare the NO<sub>2</sub> diurnal cycles observed by GEMS over the Seoul and Beijing metropolitan areas in winter and summer. We compare to the diurnal cycles observed by Pandora in the urban cores and to simulations with the GEOS-Chem CTM. We use GEOS-Chem to separate and quantify the roles of emission, chemistry, and transport in driving the NO<sub>2</sub> diurnal cycles observed from GEMS over different spatial scales. This work provides a basis for more quantitative application of GEMS observations as top-down information on NO<sub>x</sub> emissions, and more generally for interpreting the diurnal cycle of NO<sub>2</sub> from geostationary orbit with application to the TEMPO instrument over North America launched in April 2023 (Zoogman et al., 2017) and the Sentinel-4 instrument over Europe to be launched in 2024 (Gulde et al., 2017).

## 2. Observations and model

### 2.1 GEMS data

GEMS is an ultraviolet-visible instrument measuring back-scattered solar spectra at 300 – 500 nm (J. Kim et al., 2020). It was launched in February 2020 in geostationary orbit at a longitude of 128.25°E. We use hourly total NO<sub>2</sub> slant column density from the GEMS L2 NO<sub>2</sub> version 2.0 product at native 3.5 × 8 km<sup>2</sup> resolution for December-February (DJF) 2021/22 and June-August (JJA) 2022 (NIER, 2023). The GEMS NO<sub>2</sub> algorithm uses differential optical absorption spectroscopy (DOAS) to fit back-scattered solar spectra within the 432 – 450 nm range (J. Kim et al., 2020). This yields the slant column density along the light path (L2 data). We use all GEMS L2 NO<sub>2</sub> version 2.0 data that pass algorithm quality flag ≤ 112,

**Deleted:** Its native pixel resolution is 3.5 × 8 km<sup>2</sup> at Seoul, with variations in Level 2 product resolutions depending on the pixel binning configurations.

final algorithm flag  $\leq 1$ , solar zenith angle (SZA)  $< 70^\circ$ , viewing zenith angle (VZA)  $< 70^\circ$ , and cloud fraction  $< 0.3$  (Lee et al., 2020).

120 The vertical column density of  $\text{NO}_2$  is obtained by dividing the slant column density by an air mass factor (AMF) characterizing the photon path from the Sun down through the atmosphere and back up to the instrument. The AMF depends on the viewing geometry and on the scattering properties of the atmosphere:

$$\text{AMF} = \text{AMF}_G \int_0^{\text{TOA}} w(z) S(z) dz \quad (1)$$

25 Here TOA is the top of the atmosphere,  $\text{AMF}_G$  is the geometric AMF defined by the solar zenith angle (SZA) and the satellite viewing angle (VZA) as  $\text{AMF}_G = \sec(\text{SZA}) + \sec(\text{VZA})$ ,  $w(z)$  is the scattering weight that defines the instrument's sensitivity to  $\text{NO}_2$  at altitude  $z$ , and  $S(z)$  is a normalized vertical profile of  $\text{NO}_2$  number density called the shape factor (Palmer et al., 2001). Scattering weights are calculated with a radiative transfer model and increase with altitude (Martin et al., 2002; Yang et al., 2023). The shape factor is usually estimated with a CTM.

30 An alternative DOAS retrieval and AMF by Lange et al. (2024) improved the GEMS L2  $\text{NO}_2$  version 2.0 vertical column density product, which was biased due to using incorrect vertical profiles for AMF computation (Oak et al., 2024). Here, we use our own AMF. We use scattering weights at 448 nm compiled as a look-up table dependent on SZA, VZA, relative azimuth angle (RAA), surface albedo, cloud top pressure, and effective cloud fraction (R. Park and Kwon, 2020). We specify the shape factor with local

35  $\text{NO}_2$  concentrations from the GEOS-Chem simulation described in Section 2.3 and extending to the mesosphere. In simulations of observations from the KORUS-AQ aircraft campaign over South Korea, Yang et al. (2023) showed that GEOS-Chem was successful in reproducing the  $\text{NO}_2$  vertical profile observed below 5 km altitude and inferred from NO observations above. They found that the PBL extending to 2 km altitude accounted for over 95% of the  $\text{NO}_2$  tropospheric column and 80-91% of the total  $\text{NO}_2$  atmospheric column in the Seoul and Beijing metropolitan areas of interest here. The model correctly simulated the observed diurnal variation of the PBL  $\text{NO}_2$  vertical profile over Seoul as driven by mixed

Deleted:  $\int_0^{\infty} w(z) S(z) dz$

Deleted: where

Deleted: typically

Deleted: Here we use scattering weights at 448 nm calculated for the application to a 435 – 461 nm spectral window

Deleted: .

Deleted: Seoul

Deleted: observed diurnal variation in the

Deleted: of  $\text{NO}_2$  as driven by PBL mixing, with important implications for

Deleted: diurnal variation in the AMF. The GEOS-Chem simulation extends vertically to the mesosphere, and we compute in this manner the AMF for the whole atmosphere to obtain a total vertical column density. The contribution of the stratosphere to the total  $\text{NO}_2$  column in GEOS-Chem is only 9- 20% for the Seoul and Beijing metropolitan areas of interest here. The

Deleted: accounts

Deleted: over the Seoul Metropolitan Area (Yang et al., 2023)....

layer growth. This resulted in a diurnal amplitude of 14% for the AMF, peaking in the afternoon when mixing depth is maximum.

## 2.2 Pandora data

The Pandora instruments measure radiance at 280 – 525 nm (Herman et al., 2018) and fit total column NO<sub>2</sub> (including the stratosphere). There were two Pandora sites in Seoul and one in Beijing (40.0°N, 116.4°E) for the 2021-2022 period. The two Pandora sites in Seoul are at Seoul National University (Seoul – SNU; 37.5°N, 127.0°E) in the southern part of Seoul (M. Kim et al., 2021; S. Park et al., 2018) and at Yonsei University (Seoul – YSU; 37.6°N, 126.9°E) in the northern part of Seoul (J. Kim., 2017). The Beijing site is located on the north side of Beijing and a more detailed description is in O. Liu et al. (2024). We obtain the Pandora direct Sun data from the Pandonia global network (PGN, 2023). We exclude low-quality data (quality flag = 12) as recommended by PGN (PGN, 2021).

## 2.3 GEOS-Chem model

We use GEOS-Chem CTM version 13.3.4 (<https://doi.org/10.5281/zenodo.5764874>) driven by assimilated meteorological data from the Goddard Earth Observing System – Forward Processing (GEOS-FP) with a horizontal resolution of 0.25° × 0.3125° (≈ 25×25 km<sup>2</sup>) over East Asia (24 – 52°N, 104 – 133°E) and 3-hourly boundary conditions from a global GEOS-Chem simulation with 4° × 5° resolution. GEOS-FP provides the finest spatial resolution available to drive GEOS-Chem. The model has 47 vertical levels including 14 vertical levels in the lower 2 km. Simulations were conducted for DJF 2021/2022 and JJA 2022 with 6 months of initialization for each period.

Aside from emissions (see below), the simulation is the same as previously described by Yang et al. (2023) and features some modifications to the standard GEOS-Chem 13.3.4 to better reproduce KORUS-AQ aircraft observations over Korea in May-June 2016. These include aerosol nitrate photolysis, volatile chemical product (VCP) emissions and chemistry, and reduced HO<sub>2</sub> uptake by aerosol.

Formatted: Indent: First line: 0.5"

Deleted: are

Deleted: ; O. Liu et al., 2023

Deleted: ) and

Deleted: with a NO<sub>2</sub>

Deleted: of

Deleted: .

Moved down [1]: Yang et al.

Deleted: (2023) showed that the model could successfully simulate NO<sub>x</sub> chemistry during KORUS-AQ including the diurnal variation of NO<sub>2</sub> vertical profiles affecting the diurnal variation of the AMF. This gives us confidence in the application of GEOS-Chem normalized vertical profiles in Eq. (1) to compute AMFs for application to the GEMS data.

Simulations for 2022 require adjustment to NO<sub>x</sub> emissions beyond the most recent emission  
inventories used in GEOS-Chem for China (MEIC for 2019; Zheng et al., 2021) and Korea (KORUSv5 for  
2015; Woo et al., 2020). We apply for this purpose the surface NO<sub>2</sub> concentration trends for China from the  
Ministry of Ecology and Environment (MEE) network (MEE, 2023) and for South Korea from the  
AirKorea network (KEC, 2023), focused mostly on urban sites. Mean 2022/2019 surface NO<sub>2</sub>  
concentration ratios in China are 0.91 in DJF and 0.83 in JJA, and mean 2022/2015 values in Korea are  
0.70 in DJF and 0.51 JJA, which are applied to scale the anthropogenic NO<sub>x</sub> emissions. We assume these  
scaling factors to be applicable to Beijing and Seoul.

Yang et al. (2023) found that the GEOS-Chem simulation during KORUS-AQ successfully  
reproduced important features of NO<sub>x</sub> chemistry, notably the NO/NO<sub>2</sub> ratio driven by photochemical  
cycling involving ozone and HO<sub>2</sub>. Several other studies have evaluated the GEOS-Chem simulation of NO<sub>x</sub>  
over East Asia. R. Park et al. (2021) found that GEOS-Chem successfully reproduced the NO<sub>x</sub> vertical  
profiles observed during KORUS-AQ. Shah et al. (2020) found a good simulation of the seasonality of  
OMI NO<sub>2</sub> over China and its long-term trend. M. Liu et al. (2018) found that NO<sub>2</sub> diurnal variability at the  
MEE stations was well captured but the model was too low, as would be expected from the urban nature of  
the sites.

#### 2.4 Diurnal variation of NO<sub>x</sub> emissions

Figure 1 shows the diurnal cycle of NO<sub>x</sub> emissions used by GEOS-Chem in Beijing and Seoul.  
MEIC for China provides monthly NO<sub>x</sub> emissions separately for the transportation, residential, industrial,  
and power sectors while KORUSv5 separates mobile, area, and point sources. Neither inventory specifies  
diurnal variations in emissions. In our work, we apply the diurnal pattern from X. Liu et al. (2019) for the  
power sector and Miao et al. (2020) for other sources in the MEIC inventory. For KORUSv5 we apply the  
diurnal pattern from X. Liu et al. (2019) for point sources, supported by results from Bae et al. (2021), and  
the industrial daily pattern from Miao et al. (2020) for area sources. We estimate the diurnal variation of

Deleted: ).

Moved (insertion) [1]

Deleted: Several previous studies aside from Yang et al. (2023)...

mobile sources in KORUSv5 using hourly Seoul Transport Operation and Information Services (TOPIS, 2023) data on weekday total traffic and construction equipment activity.

Figure 1 shows that emissions are dominated by industrial and transport sources in Beijing, and by mobile (transport) sources in Seoul. Both sectors show a broad maximum between 7 and 18 LT that defines the overall diurnal cycle of emissions and is similar in winter and summer. There are no significant rush hour peaks in transport emissions, suggesting that the surface NO<sub>2</sub> maxima observed in early morning and evening are driven more by shallow mixing depths (Moutinho et al., 2020). Total NO<sub>x</sub> emission in Beijing in winter is 30% greater than in summer, driven by the industrial source and possibly due to workplace heating. There is less seasonal variation in Seoul where mobile sources are the largest emitters.

### 3. Intercomparison of total NO<sub>2</sub> columns

Figure 2 shows the total NO<sub>2</sub> columns over eastern China and South Korea observed by GEMS and simulated by GEOS-Chem during DJF 2021/22 and JJA 2022. The GEMS data are mapped on the 0.25° × 0.3125° GEOS-Chem grid. The yellow box delineates the Seoul Metropolitan Area (SMA). The zoomed-in black boxes are Beijing and Seoul and the white boxes are the city centers where Pandora stations are located. The [maximum NO<sub>2</sub> concentrations are in the city centers in summer but are shifted to the south in winter](#) due to the prevailing winds and the long NO<sub>x</sub> lifetime (Seo et al, 2021). We see from Figure 2 that GEMS and GEOS-Chem have consistent spatial distributions and backgrounds, but GEOS-Chem over polluted regions is generally higher than GEMS except for Seoul in winter.

Figure 3 further intercompares GEOS-Chem and GEMS using the Pandora stations in Beijing and Seoul as evaluation metric. [Previous GEMS evaluation with Pandora at the native pixel resolution of GEMS was presented by S. Kim et al. \(2023\). Here we conduct the evaluation on the coarser 0.25° × 0.3125° GEOS-Chem grid as most relevant for our work.](#) GEMS and GEOS-Chem reproduce the diurnal and day-to-day variability observed by Pandora in DJF ( $R^2 = 0.87-0.90$ ) and JJA ( $R^2 = 0.77-0.79$ ). NO<sub>2</sub> column magnitudes also agree well with Pandora in winter, with linear regression slopes of 0.94 for GEMS

Deleted: plume location in winter is



and 0.90 for GEOS-Chem. Summer shows larger biases reflecting differences between the SNU and YSU Pandora sites that cannot be resolved at the  $0.25^\circ \times 0.3125^\circ$  resolution of GEOS-Chem (there are few observations at the Beijing site in JJA). YSU is more polluted than SNU, which is in a mountainous area more remote from emissions. Overall, comparison to Pandora supports the diurnal and day-to-day variability seen in the GEMS and GEOS-Chem data. The rest of our analysis focuses on the diurnal variability.

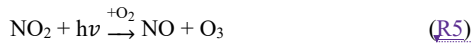
#### 4. Diurnal variation of NO<sub>2</sub> columns on the urban scale

We start with an urban core analysis focusing on the white boxes shown in Figure 2 for Beijing and Seoul, representing single  $0.25^\circ \times 0.3125^\circ$  GEOS-Chem grid cells where the Pandora stations are located.

Scatterplot comparisons between GEOS-Chem, GEMS, and Pandora for these grid cells were shown in Figure 3. Figure 4 shows the diurnal variation of the total NO<sub>2</sub> column observed from GEMS and Pandora and simulated by GEOS-Chem in Beijing. GEOS-Chem results are shown as averages for all days and for the subset of days when GEMS observations are available (generally limited by cloud cover). Wintertime NO<sub>2</sub> in all three datasets is flat from 10 to 11 LT and then increases from 11 to 14 LT. Summertime NO<sub>2</sub> decreases from 8 LT to a minimum at 13-14 LT and then increases to 16 LT, consistent between GEOS-Chem and GEMS. Pandora observations in the summertime are too limited to show.

We used the GEOS-Chem budget tendency diagnostic to understand the drivers of the diurnal variation in NO<sub>2</sub> columns. This diagnostic tracks the mean mass-weighted changes of column concentrations after each model operation for any selected horizontal domain, vertical column, and time period. We focus on the PBL column conservatively defined as extending to 3 km altitude after verifying that altitudes higher than 3 km make negligible contributions to diurnal changes in the total model column. Within the PBL column we consider the budget of NO<sub>2</sub> as that of NO<sub>x</sub> ( $\equiv \text{NO} + \text{NO}_2 + \text{NO}_3 + 2\text{N}_2\text{O}_5 + \text{HONO} + \text{HNO}_4 + \text{ClONO}_2$ ) multiplied by the local NO<sub>2</sub>/NO<sub>x</sub> PBL column concentration ratio. This eliminates from the budget the fast interconversion reactions within the NO<sub>x</sub> family and provides a more

useful budget perspective. It allows us to consider NO<sub>x</sub> emission as a source of NO<sub>2</sub> even though NO<sub>x</sub> is emitted mainly as NO. The NO<sub>x</sub> family is mainly contributed by NO and NO<sub>2</sub>, and the main interconversion reactions defining the NO<sub>2</sub>/NO<sub>x</sub> ratio are



where RO<sub>2</sub> denotes organic peroxy radicals and X denotes halogen atoms. The net tendency for the PBL NO<sub>2</sub> column ( $\Omega_{\text{NO}_2}$ ) can then be related to that of NO<sub>x</sub> ( $\Omega_{\text{NO}_x}$ ) as

$$\left[ \frac{\partial \Omega_{\text{NO}_2}}{\partial t} \right]_{\text{net}} = \alpha(t) \left[ \frac{\partial \Omega_{\text{NO}_x}}{\partial t} \right]_{\text{net}} \quad (2)$$

with

$$\left[ \frac{\partial \Omega_{\text{NO}_x}}{\partial t} \right]_{\text{net}} = \left[ \frac{\partial \Omega_{\text{NO}_x}}{\partial t} \right]_{\text{emission}} + \left[ \frac{\partial \Omega_{\text{NO}_x}}{\partial t} \right]_{\text{chemistry}} + \left[ \frac{\partial \Omega_{\text{NO}_x}}{\partial t} \right]_{\text{transport}} \quad (3)$$

and where  $\alpha(t) = \Omega_{\text{NO}_2} / \Omega_{\text{NO}_x}$  is the NO<sub>2</sub>/NO<sub>x</sub> PBL column ratio. The terms on the right-hand side of Eq. (3) are updated by GEOS-Chem over its operator splitting time steps and are archived in the budget diagnostic as spatial and temporal averages. NO<sub>x</sub> dry deposition is included in the emission operator, but its contribution is very small (Shah et al., 2020).  $\alpha(t)$  is archived every hour for application in Eq. (2).

The second row of Figure 4 shows the different NO<sub>x</sub> budget terms from Eq. (3) over hourly time steps, with the net tendency as the left-hand-side term. The third row shows the NO<sub>2</sub>/NO<sub>x</sub> PBL column molar ratios in GEOS-Chem. Each data point in the second and third rows (centered on the half hour) explains the change between the two successive hours shown in the first row. The GEOS-Chem diurnal variation in the NO<sub>2</sub> column in the first row reflects the net NO<sub>x</sub> tendency combined with the NO<sub>2</sub>/NO<sub>x</sub> ratio. We see that the increase in the NO<sub>2</sub> column over the course of the day in winter reflects the dominant effect of daytime emissions, four times higher than at night and leading to NO<sub>x</sub> accumulation. Chemical loss is slow in winter and transport (flux divergence) is the main loss term. The flat trend of the NO<sub>2</sub>

Deleted: R3

Deleted: The differential net budget

Formatted: Justified, Line spacing: 1.5 lines

Deleted: In this manner, we

column from 10 to 11 LT corresponds to the diurnal minimum of the  $\text{NO}_2/\text{NO}_x$  ratio. This ratio increases over the rest of the day as the mixed layer deepens and the freshly emitted NO is exposed to higher ozone concentrations. The increase in the ratio contributes to the increase in the  $\text{NO}_2$  column. The  $\text{NO}_2$  column in GEOS-Chem thus peaks at 18 LT. During the night, the  $\text{NO}_x$  emission decreases and the loss from transport leads to decrease in the total  $\text{NO}_2$  column. The  $\text{NO}_2/\text{NO}_x$  ratio at night is only  $0.55 \text{ mol mol}^{-1}$ , despite no  $\text{NO}_2$  photolysis, because of sustained NO emission and the slow rate of the  $\text{NO} + \text{O}_3$  reaction (low ozone and low temperatures).

The opposite diurnal variation of  $\text{NO}_2$  in summer reflects weaker daytime emission of  $\text{NO}_x$  and stronger chemical loss as shown by the GEOS-Chem budget analysis. Even though the emission term remains larger than the chemical loss term, there is also a negative transport term from ventilation. The chemical loss of  $\text{NO}_x$  peaks at 11-12 LT and then weakens, reflecting the noon maximum of OH concentrations (Logan et al., 1981) combined with the decreasing  $\text{NO}_2$  concentration, and explaining the slow recovery of the  $\text{NO}_2$  column in the afternoon. The  $\text{NO}_2/\text{NO}_x$  ratio is higher in summer than in winter and shows little variation during the daytime, reflecting the higher concentrations of  $\text{O}_3$  and  $\text{HO}_2$  radicals offsetting the effect of  $\text{NO}_2$  photolysis. The daytime  $\text{NO}_2/\text{NO}_x$  ratio averages  $0.75 \text{ mol mol}^{-1}$  in summer, as compared to  $0.50 \text{ mol mol}^{-1}$  in winter, contributing to the seasonality of  $\text{NO}_2$  seen from space.

Figure 5 shows the same as Figure 4 but for Seoul. The two Pandora stations show differences in  $\text{NO}_2$  columns, particularly in summer, as previously shown in Figure 3. They also show some differences in diurnal variation, particularly in winter, which we similarly attribute to local effects such as different emissions, wind speeds, and geography that cannot be resolved at 25-km resolution. The diurnal variations of GEMS and GEOS-Chem agree to within the ranges defined by data from the two Pandora stations.  $\text{NO}_2$  columns in winter increase from 10 to 12 LT as in Beijing but then flatten in the afternoon, which we attribute in GEOS-Chem to stronger winds.  $\text{NO}_2$  columns in summer show an increase from 8 to 10 LT, unlike in Beijing, because of larger emissions initially overwhelming the chemical loss term. There follows

**Deleted:** because upwind emissions are much lower. Without the transport loss term, the  $\text{NO}_2$  column in summer would still increase over the course of the day.

**Deleted:** 5

**Deleted:** 2

**Deleted:** data

a decrease until 13-14 LT and a recovery in the later afternoon, similar to Beijing and driven by the same factors.

### 5. Separating the influences of emission, chemistry, and transport

We showed in Section 4 that the diurnal variation of the NO<sub>2</sub> column observed by GEMS on the urban scale reflects a balance between emission and transport in winter, and the added influence from chemical loss in summer. The transport term can be represented with a CTM in an inversion framework (Cooper et al., 2017), but simple quantification of the transport term on the urban scale can also be done from knowledge of the wind speed with a mass balance approach (Jacob et al., 2016).

Figure 6 illustrates the sensitivity of the NO<sub>2</sub> diurnal variation to wind speed in the wintertime GEMS observations over Seoul when chemical loss is a negligible term. A wind speed of 6 m s<sup>-1</sup> ventilates the 25×25 km<sup>2</sup> urban core on a time scale of one hour. Here we segregate the data by GEOS-FP hourly wind speed at 850 hPa higher or lower than 6 m s<sup>-1</sup>. The diurnal variations are very different at high and low wind speed, and consistent between GEMS and GEOS-Chem. At high wind speed, the NO<sub>2</sub> column shows little diurnal variability because emission is balanced by transport. At low wind speed, NO<sub>2</sub> accumulates over the daytime hours because the transport term is weaker and does not keep up with emissions. Steady state between emissions and ventilation is finally reached at 16 LT but the NO<sub>2</sub> column keeps increasing until 18 LT because of increasing NO<sub>2</sub>/NO<sub>x</sub> ratio. Edwards et al. (2024) found an anticorrelation between the wind speed and tropospheric NO<sub>2</sub> column concentrations consistent with our findings.

One can reduce the effect of transport by spatial averaging over a large domain, thereby increasing the ventilation timescale. Edwards et al. (2024) showed that regionally averaging the data over Northeast Asia minimized the transport effect, though the interpretation of the result is more complicated due to averaging over diverse emission and chemical environments. Figure 7 shows the average diurnal pattern of the NO<sub>2</sub> column observed by GEMS and simulated by GEOS-Chem on the ≈150-km scale of the SMA

Deleted: This suggests that emission and chemical loss can be independently inferred from the GEMS observations in winter and summer if the role of transport can be quantified.

Deleted: are segregated

Deleted: (6 m s<sup>-1</sup>)

Deleted: from NASA GEOS-FP meteorology

Deleted: throughout

Deleted: day

Deleted: But the transport term is not negligible even at low wind speed; for a 3 m s<sup>-1</sup> wind, the

Deleted: time scale for the 25-km urban domain is only 2 hours. This also explains why the transport term remains important in summer (Figures 4 and 5), as the timescale for

Deleted: chemical loss is about 6 hours (Shah

Deleted: ., 2020).

Formatted: Font color: Text 1, Pattern: Clear (White)

(Figure 2) in winter and summer. Again, the diurnal variations observed by GEMS and simulated by GEOS-Chem are consistent. NO<sub>2</sub> columns in winter increase over the course of the day in a more regular manner than on the 25-km urban scale (Figure 5a) because the transport loss term is steadier and responds mainly to the change in the NO<sub>2</sub> column. The chemical loss term is not negligible, unlike on the urban scale, because its timescale of about 20 hours is comparable to that of transport.

Deleted: 5

Deleted: 24

We see from Figure 7 that the transport term can be successfully marginalized on the scale of the SMA in summer because the chemical loss term is faster. The resulting SMA diurnal pattern of the total NO<sub>2</sub> column is consistent with that of Seoul (Fig. 5b) but with a flatter shape and the early-afternoon minimum now driven mainly by chemistry. The amplitude is greatly dampened because emissions are five times weaker when averaged over the SMA regional domain, and because the chemical loss integrates over the residence time within the domain.

## 6. Conclusions

We used the GEOS-Chem model to interpret the diurnal variation of NO<sub>2</sub> columns observed from the GEMS geostationary instrument and Pandora ground-based spectrometers over Beijing and Seoul in December-January-February (DJF) 2021/22 and June-July-August (JJA) 2022. This was motivated by the need to understand the unique information offered by hourly geostationary satellite observations on the budget of NO<sub>x</sub> through the contributions of emissions, chemistry, and transport to the diurnal cycle of NO<sub>2</sub>.

Deleted: East Asia

The GEOS-Chem model used in this work had previously shown successful simulation of the NO<sub>2</sub> vertical profile and its diurnal variation over Seoul in the KORUS-AQ aircraft campaign, enabling reliable computation of the diurnal dependence of the air mass factor (AMF) that contributes to the diurnal variation of NO<sub>2</sub> observed from space. Here we used the diagnostic budget capability in GEOS-Chem to isolate the contributions of NO<sub>x</sub> emissions, chemistry, transport, and the NO<sub>2</sub>/NO<sub>x</sub> column ratio to the diurnal cycle of NO<sub>2</sub> columns. We also updated NO<sub>x</sub> emissions to 2022 including their diurnal variations. The NO<sub>x</sub> emissions for Beijing and Seoul are a factor of four higher in the daytime than at night, reflecting

Deleted: resolving

mobile and industrial sources, and show little variation during the daytime hours. We focused on simulation of the total atmospheric NO<sub>2</sub> column rather than the tropospheric column, taking advantage of the stratospheric capability in GEOS-Chem, to avoid errors in the definition of the tropopause. Diurnal variation of the NO<sub>2</sub> atmospheric column in the two cities is mainly determined by the planetary boundary layer (PBL) up to 3 km altitude.

Deleted: and

We investigated the diurnal variation of the NO<sub>2</sub> column at the 25-km urban scale over Beijing and Seoul. GEMS, Pandora, and GEOS-Chem show similar variability and diurnal variations. NO<sub>2</sub> columns in winter increase over the course of the daytime hours, reflecting accumulation from high daytime emissions offset by loss from horizontal transport (flux divergence), and further enhanced by increase in the NO<sub>2</sub>/NO<sub>x</sub> over the course of the day as ozone is entrained in the growing mixed layer. Chemical loss of NO<sub>x</sub> in winter is too slow to play a significant role in the observed diurnal variation. In summer, by contrast, NO<sub>2</sub> columns decrease from 10 to 14 local time (LT) because of NO<sub>x</sub> photochemical oxidation compounding the loss from transport.

**Deleted:** The NO<sub>2</sub> column would still increase throughout the day in summer as in winter were it not for the loss from transport. ¶  
Our results indicate that the diurnal variation of NO<sub>2</sub> column observed from geostationary orbit can be used to quantify urban NO<sub>x</sub> emissions in winter, and chemical loss in summer, but the transport term must be accounted for. This can be done by simple mass balance using knowledge of the local wind speed or by an inversion with a full CTM.

We further examined the importance of transport for interpreting the diurnal variation in the GEMS urban NO<sub>2</sub> data by segregating the Seoul data by wind speed. In winter, the low-wind GEMS data (< 6 m s<sup>-1</sup>) show steady rise of NO<sub>2</sub> over the course of the day while the high-wind data (≥ 6 m s<sup>-1</sup>) show flat diurnal variation, consistent with the GEOS-Chem model. Transport plays an important role in the NO<sub>x</sub> budget in both cases but cannot keep up with the high daytime emissions in the low-wind case.

Deleted: the

Deleted:

We examined whether the role of transport in the diurnal variation of the urban NO<sub>2</sub> column could be reduced by spatial averaging of the data over the 150-km regional scale of the Seoul Metropolitan Area (SMA). The SMA data in winter show a steady increase over the daytime hours due to emissions, but the transport term remains the major sink of NO<sub>x</sub>. The SMA data in summer show negligible loss from transport in daytime because chemical loss term is much faster, but the diurnal amplitude is weak because of diluted emissions and long residence times for the air over the regional domain.

Our conclusions regarding the interpretation of the diurnal variation of NO<sub>2</sub> columns observed by GEMS can be extended to other instruments of the geostationary air quality constellation, such as TEMPO over North America, launched in April 2023 and Sentinel-4 over Europe, scheduled for launch in 2024.

440 This work further lays the groundwork for use of GEOS-Chem in inversions of the geostationary satellite data to infer NO<sub>x</sub> emissions.

#### **Code Availability**

The model code used in this work is available at <https://doi.org/10.5281/zenodo.5764874> (The International GEOS-Chem User Community, 2021).

#### **Data availability**

445 The GEMS L2 NO<sub>2</sub> v2.0 slant column data can be obtained with a request to the NIER GEMS team (NIER, 2023). The total NO<sub>2</sub> columns from Pandora are available from the Pandonia Global Network website (<http://pandonia-global-network.org>; PGN, 2023). The surface NO<sub>2</sub> data over China are available from <https://quotsoft.net/air/> (MEE, 2023). The surface NO<sub>2</sub> data over South Korea are from AirKorea website  
450 (<https://www.airkorea.or.kr>; KEC, 2023). The Seoul hourly traffic count data is available from the Seoul Transport Operation and Information Services website (<https://topis.seoul.go.kr/>; TOPIS, 2023).

#### **Acknowledgements**

This material is based upon work supported by the National Science Foundation Graduate Research Fellowship under grant no. DGE 2140743. [We thank A. G. Russell for helpful discussions.](#)

#### **Author contribution**

455 The original draft preparation was done by LHY, with review and editing by DJJ, KRT, JHC, HL, and JK. DJJ contributed to project conceptualization. Modeling was done by LHY with additional support from HPL, NKC, SZ, VS, EB, XF, RMY, and DCP. The formal analysis was conducted by LHY with additional support from DJJ, RD, YJO, HC, JP, HLL, WJL, SK, EK, KRT, and JHC.

#### **Competing Interests**

The contact author has declared that none of the authors has any competing interests.

### Financial support

This work was funded by the Samsung PM2.5 Strategic Research Program and by the Harvard-NUIST Joint Laboratory for Air Quality and Climate (JLAQC).

- Deleted: research
- Deleted: supported
- Deleted: Advanced Institute of Technology
- Deleted: Nanjing University of Information Science
- Deleted: Technology.

### References

Bae, M., Yoo, C., Kim, H., and Kim, S.: Developing Temporal Allocation Profiles for Electric Generating Utilities based on the CleanSYS Real-time Emissions, *J. Korean Soc. Atmos.*, 37, 338–354, <https://doi.org/10.5572/KOSAE.2021.37.2.338>, 2021.

Boersma, K. F., Jacob, D. J., Eskes, H. J., Pinder, R. W., Wang, J., and van der A, R. J.: Intercomparison of SCIAMACHY and OMI tropospheric NO<sub>2</sub> columns: Observing the diurnal evolution of chemistry and emissions from space, *J. Geophys. Res.*, 113, 2007JD008816, <https://doi.org/10.1029/2007JD008816>, 2008.

Boersma, K. F., Jacob, D. J., Trainic, M., Rudich, Y., DeSmedt, I., Dirksen, R., and Eskes, H. J.: Validation of urban NO<sub>2</sub> concentrations and their diurnal and seasonal variations observed from the SCIAMACHY and OMI sensors using in situ surface measurements in Israeli cities, *Atmos. Chem. Phys.*, 9, 3867–3879, <https://doi.org/10.5194/acp-9-3867-2009>, 2009.

Chang, L.-S., Kim, D., Hong, H., Kim, D.-R., Yu, J.-A., Lee, K., Lee, H., Kim, D., Hong, J., Jo, H.-Y., and Kim, C.-H.: Evaluation of correlated Pandora column NO<sub>2</sub> and in situ surface NO<sub>2</sub> measurements during GMAP campaign, *Atmos. Chem. Phys.*, 22, 10703–10720, <https://doi.org/10.5194/acp-22-10703-2022>, 2022.

Cheng, N., Li, Y., Sun, F., Chen, C., Wang, B., Li, Q., Wei, P., and Cheng, B.: Ground-Level NO<sub>2</sub> in Urban Beijing: Trends, Distribution, and Effects of Emission Reduction Measures, *Aerosol Air Qual. Res.*, 18, 343–356, <https://doi.org/10.4209/aaqr.2017.02.0092>, 2018.

Cooper, M., Martin, R. V., Padmanabhan, A., and Henze, D. K.: Comparing mass balance and adjoint methods for inverse modeling of nitrogen dioxide columns for global nitrogen oxide emissions, *JGR Atmospheres*, 122, 4718–4734, <https://doi.org/10.1002/2016JD025985>, 2017.

Crawford, J. H., Ahn, J.-Y., Al-Saadi, J., Chang, L., Emmons, L. K., Kim, J., Lee, G., Park, J.-H., Park, R. J., Woo, J. H., Song, C.-K., Hong, J.-H., Hong, Y.-D., Lefer, B. L., Lee, M., Lee, T., Kim, S., Min, K.-E., Yum, S. S., Shin, H. J., Kim, Y.-W., Choi, J.-S., Park, J.-S., Szykman, J. J., Long, R. W., Jordan, C. E., Simpson, I. J., Fried, A., Dibb, J. E., Cho, S., and Kim, Y. P.: The Korea–United States Air Quality (KORUS-AQ) field study, *Elementa: Science of the Anthropocene*, 9, 00163, <https://doi.org/10.1525/elementa.2020.00163>, 2021.

Edwards, D. P., Martínez-Alonso, S., Jo, D. S., Ortega, I., Emmons, L. K., Orlando, J. J., Worden, H. M., Kim, J., Lee, H., Park, J., and Hong, H.: Quantifying the diurnal variation of atmospheric NO<sub>2</sub> from observations of the Geostationary Environment Monitoring Spectrometer (GEMS), *EGUsphere [preprint]*, <https://doi.org/10.5194/egusphere-2024-570>, 2024.

Ghude, S. D., Karumuri, R. K., Jena, C., Kulkarni, R., Pfister, G. G., Sajjan, V. S., Pithani, P., Debnath, S., Kumar, R., Upendra, B., Kulkarni, S. H., Lal, D. M., Vander A, R. J., and Mahajan, A. S.: What is driving the diurnal variation in tropospheric NO<sub>2</sub> columns over a cluster of high emission thermal power plants in India?, *Atmospheric Environment: X*, 5, 100058, <https://doi.org/10.1016/j.aeaoa.2019.100058>, 2020.

Gulde, S. T., Kolm, M. G., Smith, D. J., Maurer, R., Courrèges-Lacoste, G. B., Sallusti, M., and Bagnasco, G.: Sentinel 4: a geostationary imaging UVN spectrometer for air quality monitoring: status of



- design, performance and development, in: International Conference on Space Optics — ICSO 2014, Tenerife, Spain, 17 November 2017, 1158–1166, <https://doi.org/10.1117/12.2304099>, 2017.
- 510 Herman, J., Cede, A., Spinei, E., Mount, G., Tzortziou, M., and Abuhassan, N.: NO<sub>2</sub> column amounts from ground-based Pandora and MFDOAS spectrometers using the direct-sun DOAS technique: Intercomparisons and application to OMI validation, *J. Geophys. Res.*, 114, 2009JD011848, <https://doi.org/10.1029/2009JD011848>, 2009.
- 515 Herman, J., Spinei, E., Fried, A., Kim, J., Kim, J., Kim, W., Cede, A., Abuhassan, N., and Segal-Rozenhaimer, M.: NO<sub>2</sub> and HCHO measurements in Korea from 2012 to 2016 from Pandora Spectrometer Instruments compared with OMI retrievals and with aircraft measurements during the KORUS-AQ campaign, *Atmos. Meas. Tech.*, 11, 4583–4603, <https://doi.org/10.5194/amt-2018-56>, 2018.
- 520 Judd, L. M., Al-Saadi, J. A., Szykman, J. J., Valin, L. C., Janz, S. J., Kowalewski, M. G., Eskes, H. J., Veeffkind, J. P., Cede, A., Mueller, M., Gebetsberger, M., Swap, R., Pierce, R. B., Nowlan, C. R., Abad, G. G., Nehrir, A., and Williams, D.: Evaluating Sentinel-5P TROPOMI tropospheric NO<sub>2</sub> column densities with airborne and Pandora spectrometers near New York City and Long Island Sound, *Atmos. Meas. Tech.*, 13, 6113–6140, <https://doi.org/10.5194/amt-13-6113-2020>, 2020.
- 525 Jacob, D. J., Turner, A. J., Maasakkers, J. D., Sheng, J., Sun, K., Liu, X., Chance, K., Aben, I., McKeever, J., and Frankenberg, C.: Satellite observations of atmospheric methane and their value for quantifying methane emissions, *Atmos. Chem. Phys.*, 16, 14371–14396, <https://doi.org/10.5194/acp-16-14371-2016>, 2016.
- Kanaya, Y., Irie, H., Takashima, H., Iwabuchi, H., Akimoto, H., Sudo, K., Gu, M., Chong, J., Kim, Y. J., Lee, H., Li, A., Si, F., Xu, J., Xie, P.-H., Liu, W.-Q., Dzhola, A., Postlyakov, O., Ivanov, V., Grechko, E., Terpugova, S., and Panchenko, M.: Long-term MAX-DOAS network observations of NO<sub>2</sub> in Russia and Asia (MADRAS) during the period 2007–2012: instrumentation, elucidation of climatology, and comparisons with OMI satellite observations and global model simulations, *Atmos. Chem. Phys.*, 14, 7909–7927, <https://doi.org/10.5194/acp-14-7909-2014>, 2014.
- 535 KEC: The Korea Environment Corporation NO<sub>2</sub> dataset in South Korea - AirKorea [dataset], <https://www.airkorea.or.kr>, 2023.
- Kendrick, C. M., Koonce, P., and George, L. A.: Diurnal and seasonal variations of NO, NO<sub>2</sub> and PM<sub>2.5</sub> mass as a function of traffic volumes alongside an urban arterial, *Atmos. Environ.*, 122, 133–141, <https://doi.org/10.1016/j.atmosenv.2015.09.019>, 2015.
- 540 Kim, H. C., Kim, S., Lee, S.-H., Kim, B.-U., and Lee, P.: Fine-Scale Columnar and Surface NO<sub>x</sub> Concentrations over South Korea: Comparison of Surface Monitors, TROPOMI, CMAQ and CAPSS Inventory, *Atmosphere*, 11, 101, <https://doi.org/10.3390/atmos11010101>, 2020.
- Kim, J., Kim, J., Cho, H.-K., Herman, J., Park, S. S., Lim, H. K., Kim, J.-H., Miyagawa, K., and Lee, Y. G.: Intercomparison of total column ozone data from the Pandora spectrophotometer with Dobson, Brewer, and OMI measurements over Seoul, Korea, *Atmos. Meas. Tech.*, 10, 3661–3676, <https://doi.org/10.5194/amt-10-3661-2017>, 2017.
- 545 Kim, J., Jeong, U., Ahn, M.-H., Kim, J. H., Park, R. J., Lee, H., Song, C. H., Choi, Y.-S., Lee, K.-H., Yoo, J.-M., Jeong, M.-J., Park, S. K., Lee, K.-M., Song, C.-K., Kim, S.-W., Kim, Y. J., Kim, S.-W., Kim, M., Go, S., Liu, X., Chance, K., Chan Miller, C., Al-Saadi, J., Veihelmann, B., Bhartia, P. K., Torres, O., Abad, G. G., Haffner, D. P., Ko, D. H., Lee, S. H., Woo, J.-H., Chong, H., Park, S. S., Nicks, D., Choi, W. J., Moon, K.-J., Cho, A., Yoon, J., Kim, S., Hong, H., Lee, K., Lee, H., Lee, S., Choi, M., Veeffkind, P., Levelt, P. F., Edwards, D. P., Kang, M., Eo, M., Bak, J., Baek, K., Kwon, H.-A., Yang, J., Park, J., Han, K. M., Kim, B.-R., Shin, H.-W., Choi, H., Lee, E., Chong, J., Cha, Y., Koo, J.-H., Irie, H., Hayashida, S., Kasai, Y., Kanaya, Y., Liu, C., Lin, J., Crawford, J. H., Carmichael, G. R., Newchurch, M. J., Lefter, B. L., Herman, J. R., Swap, R. J., Lau, A. K. H., Kurosu, T. P., Jaross, G., Ahlers, B., Dobber, M., McElroy, C. T., and Choi, Y.: New Era of Air

- Quality Monitoring from Space: Geostationary Environment Monitoring Spectrometer (GEMS), *B. Am. Meteorol. Soc.*, 101, E1–E22, <https://doi.org/10.1175/BAMS-D-18-0013.1>, 2020.
- 560 Kim, M.-H., Yeo, H., Park, S., Park, D.-H., Omar, A., Nishizawa, T., Shimizu, A., and Kim, S.-W.: Assessing CALIOP-Derived Planetary Boundary Layer Height Using Ground-Based Lidar, *Remote Sens.*, 13, 1496, <https://doi.org/10.3390/rs13081496>, 2021.
- Kim, S., Kim, D., Hong, H., Chang, L.-S., Lee, H., Kim, D.-R., Kim, D., Yu, J.-A., Lee, D., Jeong, U., Song, C.-K., Kim, S.-W., Park, S. S., Kim, J., Hanisco, T. F., Park, J., Choi, W., and Lee, K.: First-time comparison between NO<sub>2</sub> vertical columns from Geostationary Environmental Monitoring Spectrometer (GEMS) and Pandora measurements, *Atmos. Meas. Tech.*, 16, 3959–3972, <https://doi.org/10.5194/amt-2023-11>, 2023.
- 565 <https://doi.org/10.5194/amt-2023-11>, 2023.
- Lange, K., Richter, A., Bösch, T., Zilker, B., Latsch, M., Behrens, L. K., Okafor, C. M., Bösch, H., Burrows, J. P., Merlaud, A., Pinardi, G., Fayt, C., Friedrich, M. M., Dimitropoulou, E., Van Roozendaal, M., Ziegler, S., Ripperger-Lukosiunaite, S., Kuhn, L., Lauster, B., Wagner, T., Hong, H., Kim, D., Chang, L.-S., Bae, K., Song, C.-K., and Lee, H.: Validation of GEMS tropospheric NO<sub>2</sub> columns and their diurnal variation with ground-based DOAS measurements, *EGUsphere [preprint]*, <https://doi.org/10.5194/egusphere-2024-617>, 2024.
- 570 Lee, H., Park, J., and Hyunkee, H.: Geostationary Environment Monitoring Spectrometer (GEMS) User’s Guide - Nitrogen Dioxide, The National Institute of Environmental Research, Republic of Korea, <https://nesc.nier.go.kr/ko/html/satellite/guide/guide.do>, 2020.
- 575 Liu, M., Lin, J., Wang, Y., Sun, Y., Zheng, B., Shao, J., Chen, L., Zheng, Y., Chen, J., Fu, T.-M., Yan, Y., Zhang, Q., and Wu, Z.: Spatiotemporal variability of NO<sub>2</sub> and PM<sub>2.5</sub> over Eastern China: observational and model analyses with a novel statistical method, *Atmos. Chem. Phys.*, 18, 12933–12952, <https://doi.org/10.5194/acp-18-12933-2018>, 2018.
- 580 Liu, O., Li, Z., Lin, Y., Fan, C., Zhang, Y., Li, K., Zhang, P., Wei, Y., Chen, T., Dong, J., and de Leeuw, G.: Evaluation of the first year of Pandora NO<sub>2</sub> measurements over Beijing and application to satellite validation, *Atmos. Meas. Tech.*, 17, 377–395, <https://doi.org/10.5194/amt-17-377-2024>, 2024.
- 585 Liu, X., Gao, X., Wu, X., Yu, W., Chen, L., Ni, R., Zhao, Y., Duan, H., Zhao, F., Chen, L., Gao, S., Xu, K., Lin, J., and Ku, A. Y.: Updated Hourly Emissions Factors for Chinese Power Plants Showing the Impact of Widespread Ultralow Emissions Technology Deployment, *Environ. Sci. Technol.*, 53, 2570–2578, <https://doi.org/10.1021/acs.est.8b07241>, 2019.
- <https://doi.org/10.1029/JC086iC08p07210>, 1981.
- 590 Logan, J., Prather, M. J., Wofsy, F. C., and McElroy, M. B.: Tropospheric chemistry: A global perspective, *J. Geophys. Res. Oceans*, 86, 7210–7254, <https://doi.org/10.1029/JC086iC08p07210>, 1981.
- NIER: The National Institute of Environmental Research of Republic of South Korea - GEMS dataset [data set], <https://nesc.nier.go.kr/>, 2023.
- Martin, R. V., Chance, K., Jacob, D. J., Kurosu, T. P., Spurr, R. J. D., Bucsela, E., Gleason, J. F., Palmer, P. I., Bey, I., Fiore, A. M., Li, Q., Yantosca, R. M., and Koелеmeijer, R. B. A.: An improved retrieval of tropospheric nitrogen dioxide from GOME, *J. Geophys. Res.*, 107, <https://doi.org/10.1029/2001JD001027>, 2002.
- 595 MEE: The Ministry of Ecology and Environment NO<sub>2</sub> dataset in China, MEE [data set], <https://quotsoft.net/air/>, 2023.
- Miao, R., Chen, Q., Zheng, Y., Cheng, X., Sun, Y., Palmer, P. I., Shrivastava, M., Guo, J., Zhang, Q., Liu, Y., Tan, Z., Ma, X., Chen, S., Zeng, L., Lu, K., and Zhang, Y.: Model bias in simulating major chemical components of PM<sub>2.5</sub> in China, *Atmos. Chem. Phys.*, 20, 12265–12284, <https://doi.org/10.5194/acp-20-12265-2020>, 2020.
- 600 Moutinho, J. L., Liang, D., Golan, R., Sarnat, S. E., Weber, R., Sarnat, J. A., and Russell, A. G.: Near-road vehicle emissions air quality monitoring for exposure modeling, *Atmos. Environ.*, 224, 117318, <https://doi.org/10.1016/j.atmosenv.2020.117318>, 2020.

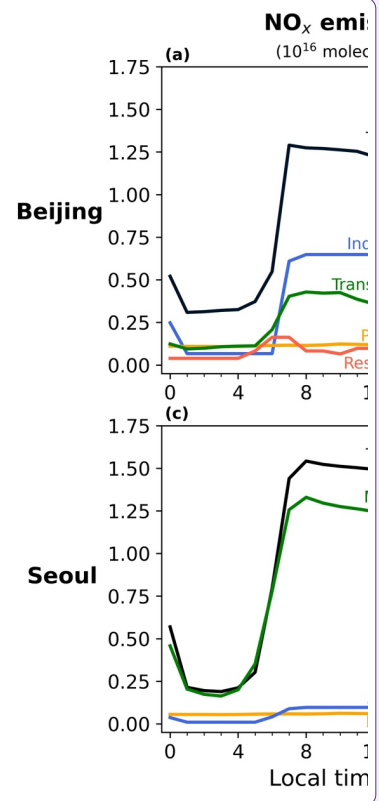
Deleted:

Formatted: Subscript

Deleted: . Discuss., 1–32, <https://doi.org/10.5194/amt-2023-177>, 2023

- 610 [Oak, Y. J., Jacob, D. J., Balasus, N., Yang, L. H., Chong, H., Park, J., Lee, H., Lee, G. T., Ha, E. S., Park, R. J., Kwon, H.-A., and Kim, J.: A bias-corrected GEMS geostationary satellite product for nitrogen dioxide using machine learning to enforce consistency with the TROPOMI satellite instrument, EGUsphere \[preprint\], <https://doi.org/10.5194/egusphere-2024-393>, 2024.](#)
- 615 Palmer, P. I., Jacob, D. J., Chance, K., Martin, R. V., Spurr, R. J. D., Kurosu, T. P., Bey, I., Yantosca, R., Fiore, A., and Li, Q.: Air mass factor formulation for spectroscopic measurements from satellites: Application to formaldehyde retrievals from the Global Ozone Monitoring Experiment, *J. Geophys. Res.*, 106, 14539–14550, <https://doi.org/10.1029/2000JD900772>, 2001.
- 620 Park, R. J. and Kwon, H.-A.: Algorithm Theoretical Basis Document - VOC (HCHO/CHOCHO) Retrieval Algorithm, The National Institute of Environmental Research, Republic of Korea, <https://nesc.nier.go.kr/en/html/satellite/doc/doc.do>, 2020.
- 625 Park, R. J., Oak, Y. J., Emmons, L. K., Kim, C.-H., Pfister, G. G., Carmichael, G. R., Saide, P. E., Cho, S.-Y., Kim, S., Woo, J.-H., Crawford, J. H., Gaubert, B., Lee, H.-J., Park, S.-Y., Jo, Y.-J., Gao, M., Tang, B., Stanier, C. O., Shin, S. S., Park, H. Y., Bae, C., and Kim, E.: Multi-model intercomparisons of air quality simulations for the KORUS-AQ campaign, *Elementa: Science of the Anthropocene*, 9, 00139, <https://doi.org/10.1525/elementa.2021.00139>, 2021.
- 630 Park, S., Kim, S.-W., Park, M.-S., and Song, C.-K.: Measurement of Planetary Boundary Layer Winds with Scanning Doppler Lidar, *Remote Sens.*, 10, 1261, <https://doi.org/10.3390/rs10081261>, 2018.
- 635 Penn, E. and Holloway, T.: Evaluating current satellite capability to observe diurnal change in nitrogen oxides in preparation for geostationary satellite missions, *Environ. Res. Lett.*, 15, 034038, <https://doi.org/10.1088/1748-9326/ab6b36>, 2020.
- 640 PGN: Pandonia Global Network (PGN) data archive [data set], <http://data.pandonia-global-network.org/>, 2023.
- 645 PGN: Pandonia Global Network (PGN) data products readme document, [https://www.pandonia-global-network.org/wp-content/uploads/2021/01/PGN\\_DataProducts\\_Readme\\_v1-8-3.pdf](https://www.pandonia-global-network.org/wp-content/uploads/2021/01/PGN_DataProducts_Readme_v1-8-3.pdf), 2021.
- 650 Seo, S., Kim, S.-W., Kim, K.-M., Lamsal, L. N., and Jin, H.: Reductions in NO<sub>2</sub> concentrations in Seoul, South Korea detected from space and ground-based monitors prior to and during the COVID-19 pandemic, *Environ. Res. Commun.*, 3, 051005, <https://doi.org/10.1088/2515-7620/abed92>, 2021.
- 655 Shah, V., Jacob, D. J., Li, K., Silvern, R. F., Zhai, S., Liu, M., Lin, J., and Zhang, Q.: Effect of changing NO<sub>2</sub> lifetime on the seasonality and long-term trends of satellite-observed tropospheric NO<sub>2</sub> columns over China, *Atmos. Chem. Phys.*, 20, 1483–1495, <https://doi.org/10.5194/acp-20-1483-2020>, 2020.
- 660 The International GEOS-Chem User Community: geoschem/GC-Classic: GEOS-Chem 13.3.4 (13.3.4), Zenodo [code], <https://doi.org/10.5281/zenodo.5764874>, 2021.
- 665 TOPIS: Seoul Transport Operation and Information Services (TOPIS) Seoul traffic count data [data set], <https://topis.seoul.go.kr/>, 2023.
- 670 Verhoelst, T., Compermolle, S., Pinardi, G., Lambert, J.-C., Eskes, H. J., Eichmann, K.-U., Fjæraa, A. M., Granville, J., Niemeijer, S., Cede, A., Tiefengraber, M., Hendrick, F., Pazmiño, A., Bais, A., Bazureau, A., Boersma, K. F., Bogner, K., Dehn, A., Donner, S., Elokhov, A., Gebetsberger, M., Goutail, F., Grutter de la Mora, M., Gruzdev, A., Gratsea, M., Hansen, G. H., Irie, H., Jepsen, N., Kanaya, Y., Karagiozidis, D., Kivi, R., Kreher, K., Levelt, P. F., Liu, C., Müller, M., Navarro Comas, M., Piters, A. J. M., Pommereau, J.-P., Portafaix, T., Prados-Roman, C., Puentedura, O., Querel, R., Remmers, J., Richter, A., Rimmer, J., Rivera Cárdenas, C., Saavedra de Miguel, L., Sinyakov, V. P., Stremme, W., Strong, K., Van Roozendaal, M., Veeffkind, J. P., Wagner, T., Wittrock, F., Yela González, M., and Zehner, C.: Ground-based validation of the Copernicus Sentinel-5P TROPOMI NO<sub>2</sub> measurements with the NDACC ZSL-DOAS, MAX-DOAS and Pandonia global networks, *Atmos. Meas. Tech.*, 14, 481–510, <https://doi.org/10.5194/amt-14-481-2021>, 2021.

- Woo, J.-H., Kim, Y., Kim, H.-K., Choi, K.-C., Eum, J.-H., Lee, J.-B., Lim, J.-H., Kim, J., and Seong, M.: Development of the CREATE Inventory in Support of Integrated Climate and Air Quality Modeling for Asia, *Sustainability*, 12, <https://doi.org/10.3390/su12197930>, 2020.
- 660 Yang, L. H., Jacob, D. J., Colombi, N. K., Zhai, S., Bates, K. H., Shah, V., Beaudry, E., Yantosca, R. M., Lin, H., Brewer, J. F., Chong, H., Travis, K. R., Crawford, J. H., Lamsal, L. N., Koo, J.-H., and Kim, J.: Tropospheric NO<sub>2</sub> vertical profiles over South Korea and their relation to oxidant chemistry: implications for geostationary satellite retrievals and the observation of NO<sub>2</sub> diurnal variation from space, *Atmos. Chem. Phys.*, 23, 2465–2481, <https://doi.org/10.5194/acp-23-2465-2023>, 2023.
- 665 Zheng, B., Zhang, Q., Geng, G., Chen, C., Shi, Q., Cui, M., Lei, Y., and He, K.: Changes in China's anthropogenic emissions and air quality during the COVID-19 pandemic in 2020, *Earth Syst. Sci. Data*, 13, 2895–2907, <https://doi.org/10.5194/essd-13-2895-2021>, 2021.
- 670 Zoogman, P., Liu, X., Suleiman, R. M., Pennington, W. F., Flittner, D. E., Al-Saadi, J. A., Hilton, B. B., Nicks, D. K., Newchurch, M. J., Carr, J. L., Janz, S. J., Andraschko, M. R., Arola, A., Baker, B. D., Canova, B. P., Chan Miller, C., Cohen, R. C., Davis, J. E., Dussault, M. E., Edwards, D. P., Fishman, J., Ghulam, A., González Abad, G., Grutter, M., Herman, J. R., Houck, J., Jacob, D. J., Joiner, J., Kerridge, B. J., Kim, J., Krotkov, N. A., Lamsal, L., Li, C., Lindfors, A., Martin, R. V., McElroy, C. T., McLinden, C., Natraj, V., Neil, D. O., Nowlan, C. R., O'Sullivan, E. J., Palmer, P. I., Pierce, R. B., Pippin, M. R., Saiz-Lopez, A., Spurr, R. J. D., Szykman, J. J., Torres, O., Veefkind, J. P., Veihelmann, B., Wang, H., Wang, J., and Chance, K.: Tropospheric emissions: Monitoring of pollution (TEMPO), *J. Quant. Spectrosc. Radiat. Transf.*, 186, 17–39, <https://doi.org/10.1016/j.jqsrt.2016.05.008>, 2017.



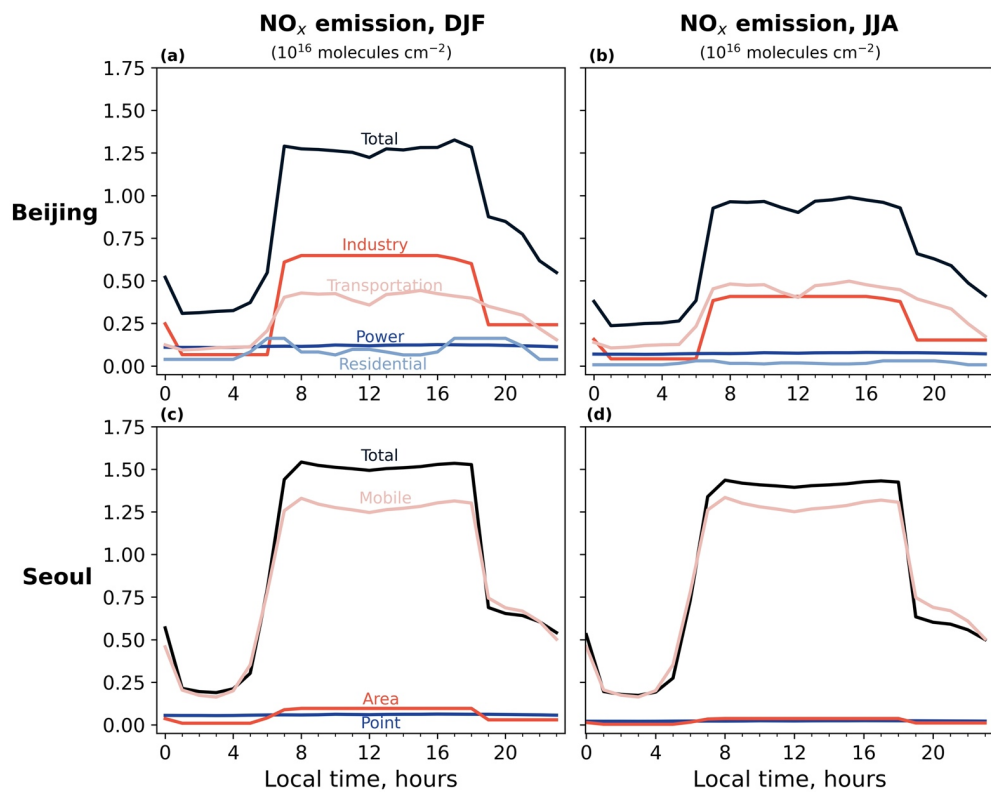


**Figure 1.** Diurnal variation of  $\text{NO}_x$  emissions in Beijing and Seoul for DJF 2021/2022 and JJA 2022. Local time is Chinese Standard Time (CST) for Beijing and Korean Standard Time (KST) for Seoul. Solar noon is at 12:08 – 12:27 CST in Beijing and 12:21 – 12:45 KST in Seoul. Values are for the white boxes in Figure 2. Different colors represent different sectors, and the black line shows the total emission.

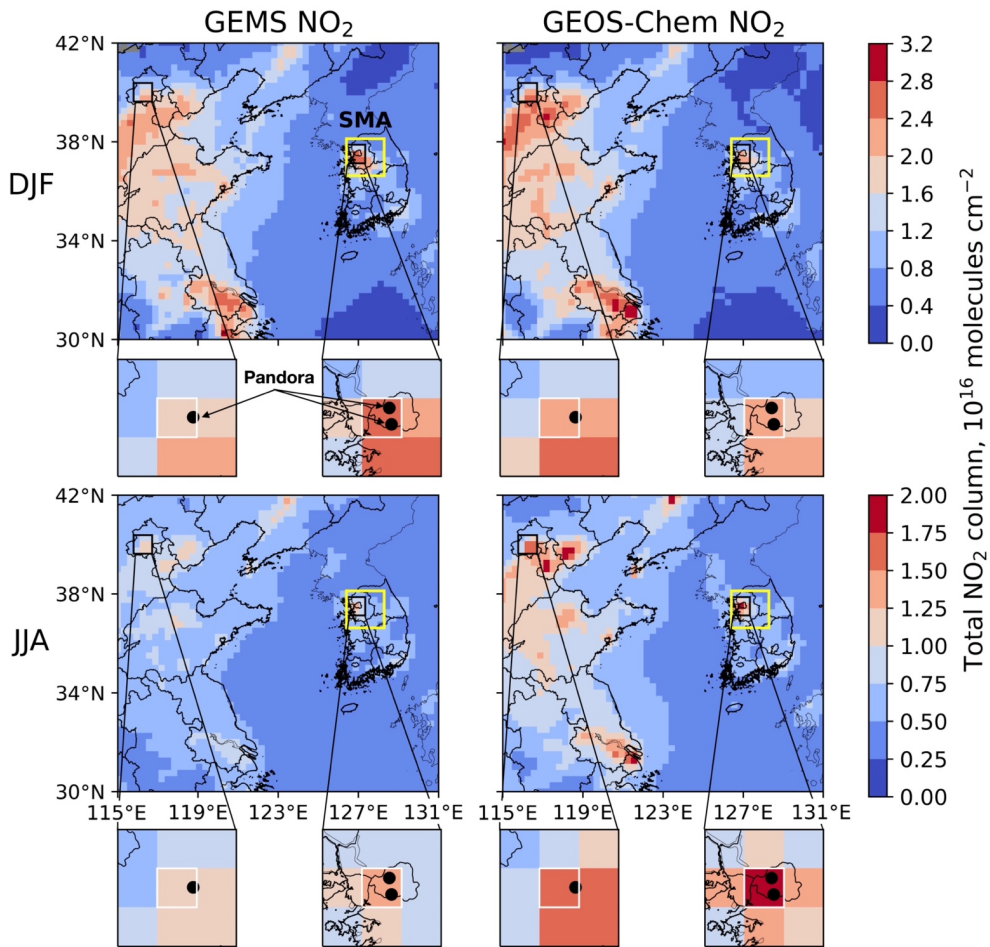


**Figure 2.** Total NO<sub>2</sub> columns over East Asia retrieved by GEMS and simulated by GEOS-Chem. The data are 3-month averages for December-January-February (DJF) 2021/22 and June-July-August (JJA) 2022 on the 0.25° × 0.3125° GEOS-Chem nested grid. The yellow rectangle delineates the Seoul Metropolitan Area (SMA; 36.6-38.1°N, 126.4-128.3°E). The zoomed-in plots show Beijing and Seoul, and the white boxes are the 0.25° × 0.3125° urban cores where the Pandora stations are located (black circles). Scales are different for DJF and JJA.

690

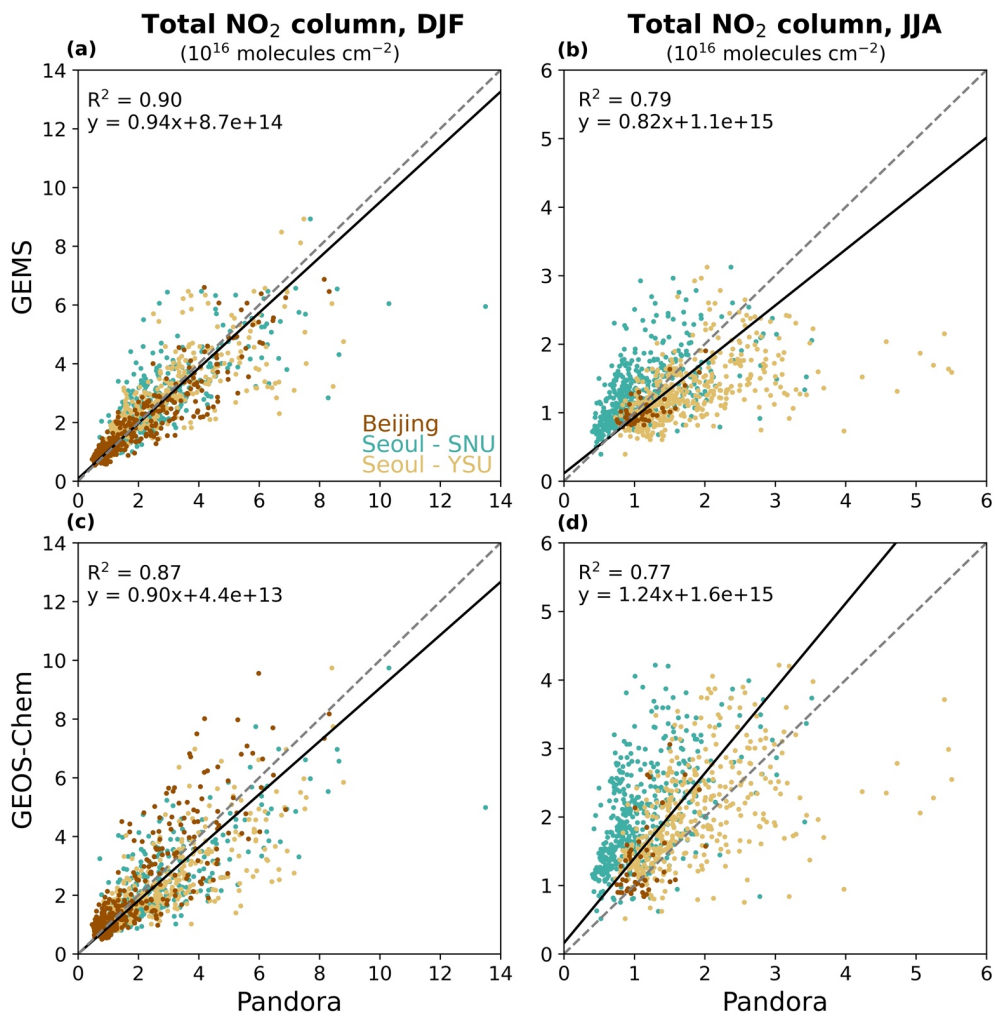


**Figure 3.** Intercomparison of GEOS-Chem, GEMS, and Pandora NO<sub>2</sub> columns for the Pandora sites in Beijing and Seoul. The Figure shows scatterplots of daytime hourly data for DJF 2021/2022 and JJA 2022. GEMS is mapped on the 0.25° × 0.3125° GEOS-Chem grid. Coefficients of determination (R<sup>2</sup>) and reduced-major axis linear regressions are shown. The 1:1 line is dashed. The Beijing Pandora site has limited observations in JJA.

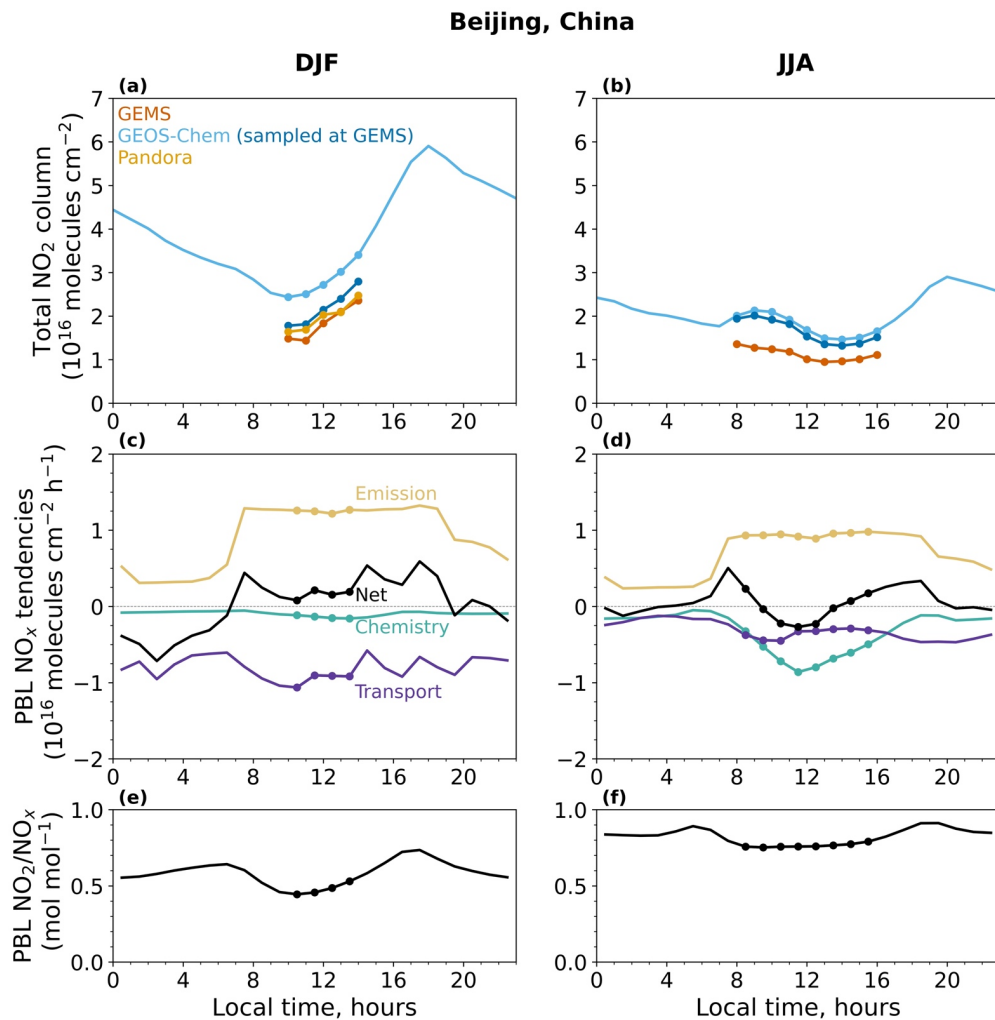


**Figure 4.** Diurnal variation of total  $\text{NO}_2$  column and driving processes in Beijing. The first row shows the average  $\text{NO}_2$  columns observed by GEMS and Pandora, and simulated by GEOS-Chem, in DJF 2021/22 and JJA 2022 for the  $0.25^\circ \times 0.3125^\circ$  GEOS-Chem grid cell in the urban core where the Pandora station is located (white box in Figure 2). GEMS observations are available for the hours indicated by symbols. GEOS-Chem results for the full diurnal cycle are shown as averages for all days and for the subset of days when GEMS data are available (generally limited by cloud cover). Pandora data are not shown for JJA due to a limited number of observations (Figure 3). The second row shows the hourly tendencies in the GEOS-Chem  $\text{NO}_x$  budget (averaged for all days) for the planetary boundary layer (PBL) conservatively defined as extending up to 3 km altitude. The tendencies describe the contributions from individual processes to the



NO<sub>x</sub> budget as given by Eq. (3), with NO<sub>x</sub> defined as NO<sub>x</sub> ≡ NO + NO<sub>2</sub> + NO<sub>3</sub> + 2N<sub>2</sub>O<sub>5</sub> + HONO + HNO<sub>4</sub> + ClNO<sub>2</sub>. The third row shows the PBL NO<sub>2</sub>/NO<sub>x</sub> column molar ratio in GEOS-Chem.

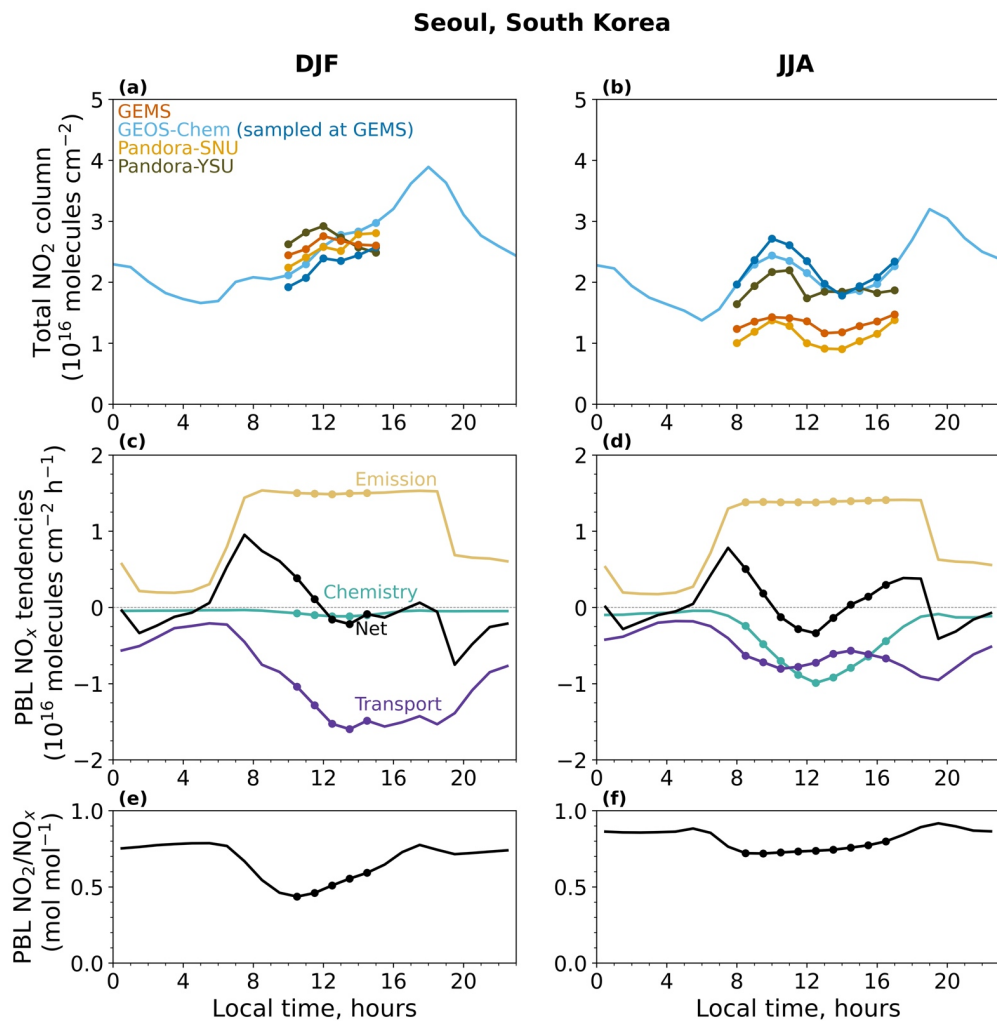


**Figure 5.** Same as Figure 4 but for Seoul.

715

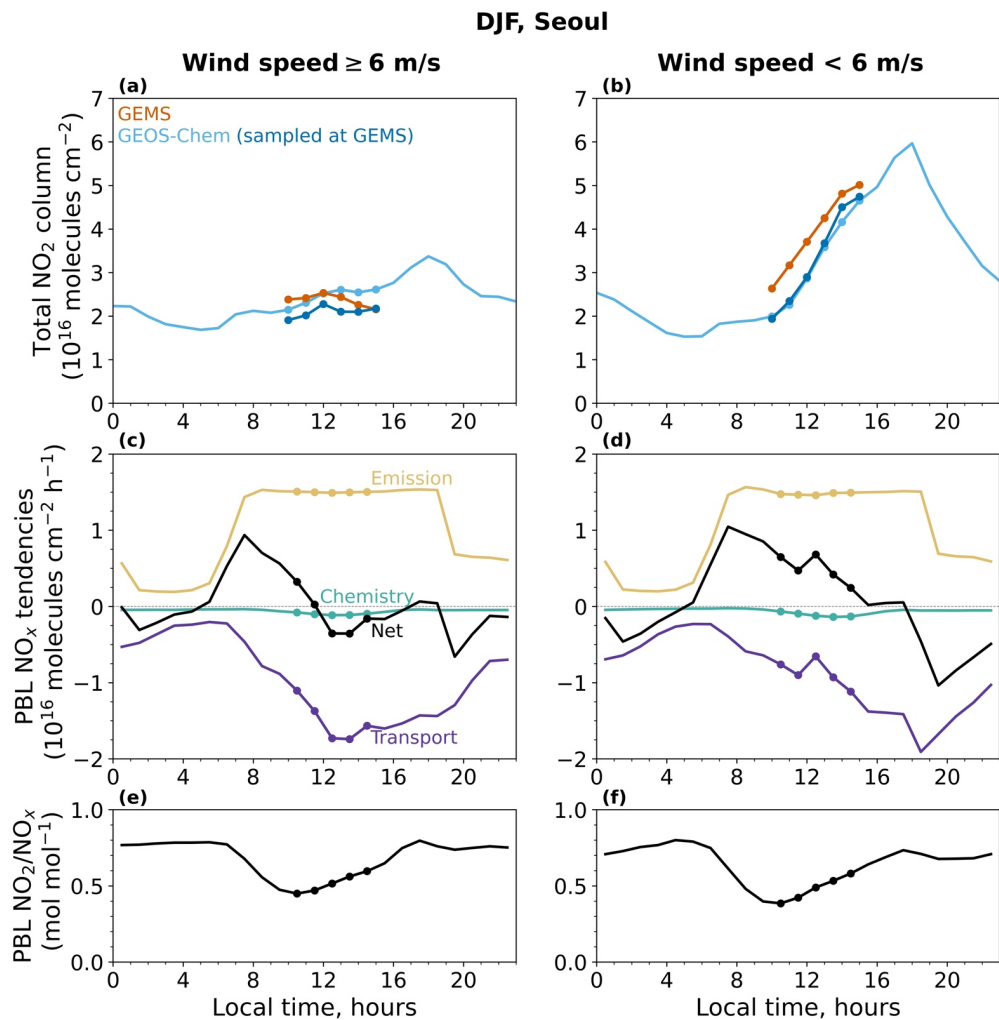


**Figure 6.** Same as Figure 4 but for DJF 2021/22 in Seoul with data segregated by wind speed. Segregation threshold is  $6 \text{ m s}^{-1}$  for the 850 hPa hourly wind speed in the NASA GEOS-FP meteorological data used as input to GEOS-Chem.

720

725

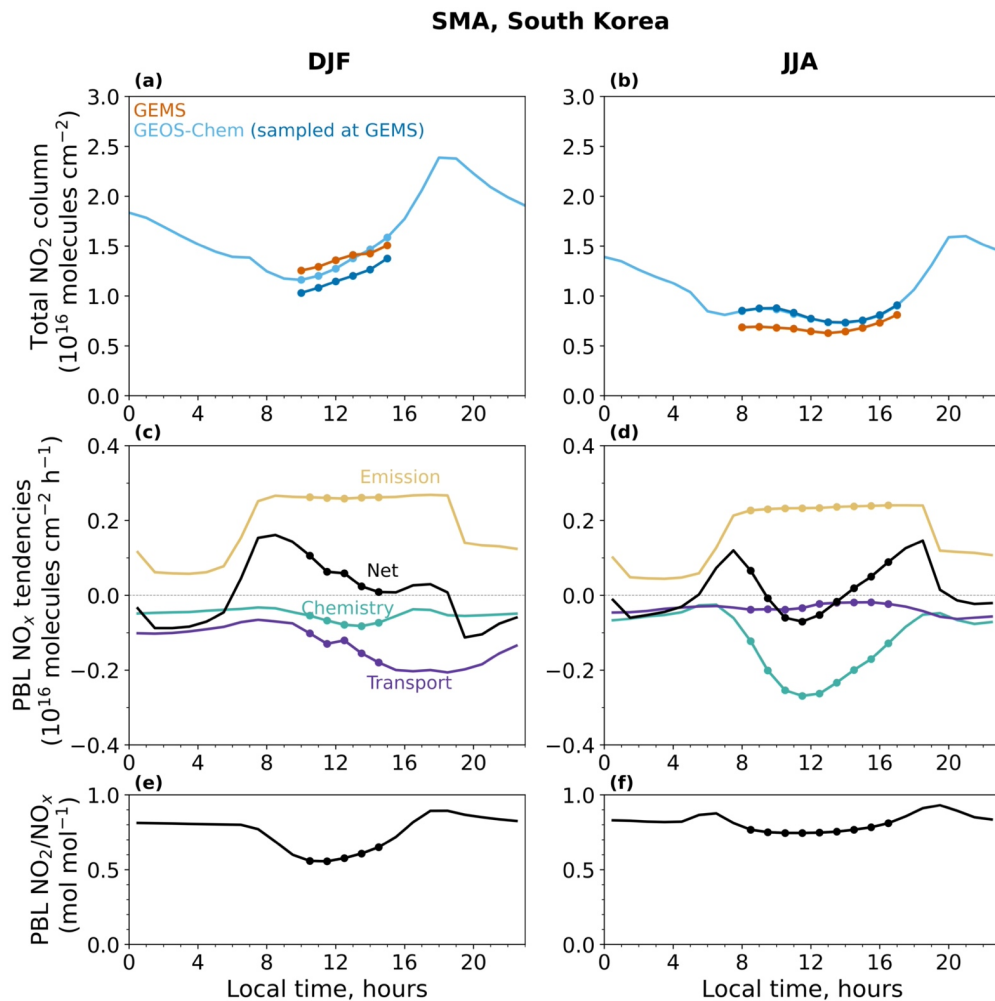


**Figure 7.** Same as for Figure 4 but for the Seoul Metropolitan Area (SMA; 36.6-38.1°N, 126.4-128.3°E) corresponding to the yellow box in Figure 2. Quantities are averages over all  $0.25^\circ \times 0.3125^\circ$  grid cells in the SMA.

Formatted: Indent: Left: 0", First line: 0"